Predictions of Structural Integrity of Steam Generator Tubes under Normal Operating, Accident, and Severe Accident Conditions*

by

Saurin Majumdar

Argonne National Laboratory
Argonne, IL 60439

October 1996

INVITED PAPER for presentation at 24th Water Reactor Safety Meeting, October 21-23, 1996, Bethesda, MD.

* Work supported by the Office of Nuclear Regulatory Research, U.S. Nuclear Regulatory Commission.

Predictions of Structural Integrity of Steam Generator Tubes under Normal Operating, Accident, and Severe Accident Conditions

Saurin Majumdar
Argonne National Laboratory
Argonne, Illinois 60439

Abstract

Available models for predicting failure of flawed and unflawed steam generator tubes under normal operating, accident, and severe accident conditions are reviewed. Tests conducted in the past, though limited, tended to show that the earlier flow-stress model for part-through-wall axial cracks overestimated the damaging influence of deep cracks. This observation was confirmed by further tests at high temperatures, as well as by finite-element analysis. A modified correlation for deep cracks can correct this shortcoming of the model. Recent tests have shown that lateral restraint can significantly increase the failure pressure of tubes with unsymmetrical circumferential cracks. This observation was confirmed by finite-element analysis. The rate-independent flow stress models that are successful at low temperatures cannot predict the rate-sensitive failure behavior of steam generator tubes at high temperatures. Therefore, a creep rupture model for predicting failure was developed and validated by tests under various temperature and pressure loadings that can occur during postulated severe accidents.

Introduction

Operating experience with PWR steam generators in both the U.S. and abroad has shown that cracks of various morphologies can and do occur in steam generator tubes, starting early in life. These may be single cracks that are axial or circumferential, ID or OD initiated, part-through-wall or through-wall, or they may be multiple cracks that are parallel or form a network. Tests have shown that, depending on the location and morphology of these cracks, the steam generator tubes can be weakened to various extents.

Under normal operating conditions, the pressure across a PWR steam generator tube wall, Δp_{no}, is ≈ 9 MPa (1300 psi); under a main steamline break (MSLB) in which the secondary side has dropped to atmospheric pressure, the pressure across the tube wall, Δp_{MSLB}, is ≈18 MPa (2560 psi). Degraded tubes must actually be capable of withstanding $3 \cdot \Delta p_{no}$ ≈27 MPa (3900 psi) and $1.4 \cdot \Delta p_{MSLB}$ ≈25 MPa (3660 psi) to meet requirements for continued operation. For typical unflawed steam generator tubes made of Alloy 600, the burst pressure, p_b, is ≈ 65 MPa (9400 psi).

Severe accidents involving significant core damage are unlikely events in nuclear reactors. Even in the unlikely event that such an accident should occur, in most cases any potential risk to the public is mitigated by the presence of a robust containment. The behavior of steam generator tubing during such severe accidents is of particular interest, since failure of the steam generator tubes could lead to bypass of the containment. As part of its effort to develop a new steam generator rule, the NRC and its contractors and EPRI have been investigating the potential for failure of steam generator tubes during severe

accidents. The accident sequences that appear to produce the greatest risk of steam generator tube failure are those in which the reactor pressure vessel fails to depressurize, but depressurization does occur on the secondary side. Even in these cases, preliminary investigations[a, b] suggest that failures are likely to occur in the hot-leg nozzle or the inlet surge-line nozzle leading to depressurization of the reactor system which prevents steam generator tube failure. However, such calculations are subject to large uncertainties and the NRC is pursuing additional studies to better understand the progression of such sequences, the temperature of the steam generator tubes during such accidents, and the behavior of steam generator tubes at the high temperatures associated with such accidents. An objective of the present work at Argonne is the development and validation of models to describe the failure of flawed steam generator tubes at high temperatures. The tests and analyses do not attempt to accurately simulate any particular severe accident scenario, rather they are intended to provide tools that can be used to determine failure under a broad range of pressure and temperature histories.

There is substantial literature[1-6] on the development and validation of analytical models to describe the behavior of flawed tubes at normal reactor operating temperatures (288–320°C). These models and data can be used to analyze the potential for failure during design basis accidents, during which the temperature of the steam generator tubing is less than 350°C. In this temperature range, creep effects are negligible in Alloy 600. However, in postulated severe accidents,[a, b] much higher temperatures are possible. At these higher temperatures, plastic deformation is likely to be much more extensive than at normal reactor operating temperatures, and creep effects can no longer be neglected. Until recently there were no test data or validated models to predict the failure of flawed tubes at temperatures associated with postulated severe accidents. Therefore, the NRC has initiated a program at ANL to generate failure data on flawed and unflawed steam generator tubes at high temperatures. The purpose of these tests was to help develop predictive models for failure of steam generator tubes under given severe accident conditions. The tests were therefore carried out to failure under various pressure and temperature histories (not necessarily simulating any particular severe accident scenario) to provide a broad data base for developing such models. A creep rupture model for failure of the remaining ligament of a part-through crack has been developed and validated by tests on tubes containing axial flaws.

All of the analytical models discussed in this paper are applicable to steam generator tubes containing a single dominant crack. Although there has been some limited analytical and experimental studies of failure of tubes containing multiple cracks, the current practice generally applies the existing models to a single enveloping crack.

Low-Temperature Failure of Tubes

Axial cracks

The critical pressures and crack sizes for the unstable failure (rupture) of a thin-wall internally pressurized cylindrical shell with a single through-wall axial crack can be estimated with an equation originally proposed by Hahn et al.[1] and later modified by Erdogan:[2]

$$p_{cr} = \frac{\bar{\sigma} h}{m R_m} = \frac{p_b}{m}, \qquad (1a)$$

where:

$$\bar{\sigma} = \text{flow stress} = k(\sigma_y + \sigma_u) \quad (\text{with } k = 0.5 - 0.6), \qquad (1b)$$

---

[a] P. G. Eilison, L. W. Ward, C. Dobbe. S. A. Chavez, C. L. Atwood, C. L. Smith, L. M. Wolfram, J. L. Jones, L. N. Haney, and W. J. Reece, The Risk Significance of Induced Steam Generator Tube Rupture, INEL-95/0641, Rev. 1 (Draft), Lockheed Martin Idaho Technologies, Inc., Idaho National Engineering Laboratory, December 15, 1995.

[b] E. L. Fuller, M. A. Kenton, M. Epstein, R. E. Henry, and N. G. Cofie, Risks from Severe Accidents Involving Steam Generator Tube Leaks or Ruptures, EPRI TR-106194, Electric Power Research Institute, Palo Alto, CA (to be published).

σ_y and σ_u are the yield and ultimate tensile strengths, respectively, (1c)

$$m = 0.614 + 0.481\lambda + 0.386\exp(-1.25\lambda), \tag{1d}$$

$$\lambda = \left[12(1-\nu^2)\right]^{\frac{1}{4}} \frac{c}{\sqrt{R_m h}} = \frac{1.82c}{\sqrt{R_m h}}, \tag{1e}$$

$$p_b = \frac{\overline{\sigma} h}{R_m} = \text{burst pressure of an unflawed virgin tubing,} \tag{1f}$$

R_m and h = mean radius and wall thickness of tube, respectively, and (1g)

2c = axial crack length. (1h)

For a single part-through axial crack, the pressure required to fail the remaining ligament can be calculated with an empirical equation (referred to as the BCL equation) reported by Kiefner et al.[4]

$$p_{sc} = \frac{\overline{\sigma} h}{m_p R_m} = \frac{p_b}{m_p}, \tag{2a}$$

where:

$$m_p = \frac{1 - \frac{a}{mh}}{1 - \frac{a}{h}}, \text{ and} \tag{2b}$$

a = axial crack depth.

Under the auspices of an NRC-sponsored steam generator tube integrity program, the Pacific Northwest National Laboratory (PNNL) conducted a series of tests on tubes containing part–through axial notches. Based on these tests, PNNL[6] developed an empirical formula for the failure pressure of a tube containing a part–through axial crack. This formula, which was later validated by testing on specimens with stress corrosion cracks, is of the same form as Eq. 2a but where Eq. 2b is replaced by:

$$m_p = \left[1 - \frac{a}{h} + \frac{a}{h}\exp(-0.41\lambda)\right]^{-1}. \tag{3a}$$

Chavez et al.[7] reanalyzed the PNNL tube test data and proposed that the value of k in Eq. 1b should be taken as 0.5973 and that Eq. 3a should be modified (referred to as the INEL equation) to:

$$m_p = \left[1 - \frac{a}{h} + \frac{a}{h}\exp(-0.51\lambda)\right]^{-1}. \tag{3b}$$

As the crack depth approaches 100% of the wal thickness (i.e., a/h = 1), Eqs. 2a-2b predict that p_{sc} approaches 0, while Eqs. 3a and 3b do not predict that p_{sc} approaches 0, i.e., they predict higher pressure for ligament failure than do Eqs. 2a-2b for short, deep cracks. Eventually, Eqs. 3a-3b would become unconservative for very deep cracks. On the other hand, Eq. 2a tends to be overly conservative for short and deep cracks. Therefore Shack[a] has re-analyzed the PNNL tube test data and proposed that Eq. 2b be modified as follows (referred to as the ANL equation):

---

[a] W.J. Shack, Argonne National Laboratory, personal communication, 1996.

$$m_p = \frac{1 - \alpha \frac{a}{mh}}{1 - \frac{a}{h}}, \qquad (2c)$$

where:

$$\alpha = 1 + 0.9\left(\frac{a}{h}\right)^2\left(1 - \frac{1}{m}\right).$$

Except for short, deep cracks, Eq. 2c predicts similar failure pressures as in Eq. 2b.

Based on burst tests on tubes, Flesch and Cochet[5] recommended the use of Eqs. 2a-b for flaw depths greater than 85% of the wall thickness. However, in order to reduce the degree of conservativetism that was apparent from comparison with experimental results, they used σ_u instead of $\bar{\sigma}$. For predicting failure of the remaining ligament by plastic instability of tubes with flaw depths between 20% and 85% of wall thickness, they recommended replacing Eq. 2b by the following empirical equation (referred to as the EDF equation):

$$m_p = \left(\frac{1 - \frac{c}{h}\frac{a}{h}}{1 + \frac{c}{h}}\right)^{-1} \quad \text{for } 0.2 < a/h < 0.85, \qquad (4a)$$

and

$$m_p = \frac{1 - \frac{a}{mh}}{1 - \frac{a}{h}} \frac{\bar{\sigma}}{\sigma_u} \quad \text{for } a/h > 0.85. \qquad (4b)$$

It should be emphasized that Eq. 2a gives only the pressure required to fail the remaining ligament. The stability of the resulting through-wall crack can be analyzed using Eq. 1a. If $p_{cr} > p_{sc}$, the through-wall crack is stable. Although the crack will leak, it will not increase in length without a further increase in pressure. If $p_{cr} < p_{sc}$, the resulting crack will be unstable and will rapidly increase in length without any additional increase in pressure.

A comparison of the values of stress magnification factor m_p as computed by the various equations is shown in Figs. 1a-b. Note that although the values of m_p as computed by the various equations are within 20-30% of each other for a shallow crack (a/h = 0.5), they can differ by as much as a factor of 2 for deep (a/h = 0.9) and short cracks (≈ 0.25 in.). Failure tests on tubes containing deep cracks (to be discussed later) have shown that the m_p values are more in accordance with the ANL equation (Eq. 2c) than the BCL equation (Eq. 2b). To verify this analytically, detailed elastoplastic finite-element analyses were conducted for a 22-mm (7/8 in.)-diameter tube with a 25-mm (1 in.) long and 50% deep axial crack and a 6-mm (0.25 in.)-long and 90% deep axial crack subjected to rapidly increasing internal pressure at 300°C and 750°C. The stress-strain curves at these temperatures are shown in Fig. 2a. The results presented in Fig. 2b show that the maximum hoop stress magnification in the ligament for the shallower crack is independent of the stress-strain curve of the material. Further, the hoop stress magnification factor (defined as the ratio of the average hoop stress in the ligament and the average hoop stress in an unflawed tube) changes very little with internal pressure and its variation with crack depth is more in agreement with the ANL equation than with the BCL equation.

Circumferential cracks

Failure loads for tubing with circumferential cracks can also be calculated by plastic limit load analyses described by Ranganath and Mehta,[8] which were based on earlier work by Kanninen et al.[9] For an unconstrained tube with a through-wall crack of angular length 2θ and no applied primary bending stress, the critical burst pressure is

$$p_{cr} = \frac{2\bar{\sigma}h}{R_m}\left(1 - \frac{\theta}{\pi} - \frac{2\beta}{\pi}\right), \tag{5a}$$

where

$$\beta = \sin^{-1}\left(\frac{\sin\theta}{2}\right) \tag{5b}$$

Limit load analyses have also been proposed for part–through cracks.[10-11]

Equation 5a is applicable to one extreme case where the tube is completely free to bend. In the opposite extreme case of total constraint against bending, a criterion based on maximum linear stress in the net section as proposed by Cochet et al.[12] can be used to calculate the instability limit pressure:

$$p_{cr} = \frac{2(\gamma^2 - 1)(\pi - \theta)\bar{\sigma}}{2\pi + (\pi - \theta)(\gamma^2 - 1)}, \tag{6a}$$

where:

$$\gamma = \frac{R_o}{R_i}. \tag{6b}$$

The following thin-shell, uniaxial approximation to Eq. 6a is often used for predicting failure of steam generator tubes that are fully constrained against bending:

$$p_{cr} = \frac{2\bar{\sigma}h}{R_m}\left(1 - \frac{\theta}{\pi}\right). \tag{6c}$$

In reality, the tube support plates offer a significant but not total restraint against bending, which tends to increase the failure pressure to somewhere between those predicted by Eqs. 5a and 6a (or 6c).

Hernalsteen[13] has developed a semiempirical approach to account for the stiffening effects of the tube support plate on the burst pressure of a steam generator tube containing a circumferential crack at the top of the tube sheet. By conducting a number of pressure tests of circumferentially flawed steam generator tube/tube sheet/tube support plate assembly and measuring the failure pressures p_{burst}, as well as the restraining loads (thus the bending moments M_{burst} at the tubesheet) at the tube support plate at burst, he developed an empirical correlation between the stress index K and the elastic rotational stiffness of the tube S, where

$$K = \frac{\left(\frac{M_{burst}}{\pi R_m^2 h} + \frac{p_{burst} R_m}{2h}\right)}{\bar{\sigma}} \tag{7a}$$

and

$$S = \frac{M}{EIy'}, \tag{7b}$$

where:

EI is the flexural stiffness of the tube, and

M and y' are the bending moment, and rotation at the tube sheet, respectively.

Based on this correlation, Hernalsteen determined the value of K from the value of S that corresponds to the steam generator tube configuration under consideration and computed the burst pressure from Eq. 7a. Typical values of K ranged from 0.6 for 2-3 m span to 0.9 for 3-4 cm span between the tube sheet and the tube support plate.

A series of elastoplastic finite-element analyses are being conducted at ANL to determine the effects of a lateral constraint on the burst pressure of a tube with a single through-wall circumferential crack. Initially, two tubes with 180° and 240° through-wall circumferential cracks were analyzed. A typical finite-element model and displacements for the free-bending case are shown in Figs. 3 a-b. Note that the beam bends almost like a rigid body about a hinge at the cracked section. Figure 4a shows the variations of the free-end displacements and the maximum rotation with the normalized burst pressure for a 180° and a 240° circumferential through-wall cracks. The displacement and rotation curves coincide, confirming that the displacement is of the rigid-body-rotation type. Both cracked tubes reach maximum pressures at a rotation of ≈ 10°. This is in agreement with the experimental observation by Hernalsteen[13] that tubes appear to fail at a fixed rotation of the cracked section. Figure 4b shows a comparison between available burst pressure data reported by Cochet and Flesch[14] and predictions by the simple beam free-bending model (Eq. 5a) and finite-element analysis. The simple model underpredicts both the test burst pressures and the finite-element results slightly. Preliminary analysis of a transversely supported tube (to simulate the tube support plate) with a 240° crack showed that the maximum pressure capability is increased significantly over that of a free-bending tube (Fig. 5a). The critical pressure for a span of 0.67 m (26 in.) appears to be much closer to the fully constrained case than the free-bending case (Fig. 5b).

High-Temperature Failure of Tubes

The behavior of flawed steam generator tubing during severe accidents has recently been considered in a report by INEL[a] and in an EPRI report.[b] In both reports, the failure of unflawed tubing and other components such as the surge line nozzle was described in terms of creep damage failure. In contrast, both analyses assumed that failure of flawed (axial crack) steam generator tubing in severe accidents can be described in terms of the models described by Eqs. 1–3 by taking the flow stress to be a function of temperature. With this assumption, the failure pressure of a flawed tube depended only on the flaw geometry and temperature and was independent of the detailed time/temperature/pressure history.

Intuitively, failure would be expected to be controlled by flow stress if the temperature ramps are sufficiently rapid so that there is insufficient time for creep to influence the deformation or damage of the tube. At the other extreme, if the temperature ramps are sufficiently slow (in the limit, a constant temperature hold), failure should be controlled by creep processes. In loading histories at intermediate rates, the damage processes are more complex and difficult to analyze.

To better understand the behavior of steam generator tubing during severe accidents, the NRC has sponsored a series of tests at ANL to help develop and validate a model for predicting failure of both flawed and unflawed steam generator tubes under such accidents. Recent tests conducted at ANL have shown that pressure and temperature ramp rates have significant influences on the failure pressure (Fig. 6a) and failure temperature (Fig. 6b), respectively. Therefore, a creep rupture model

---

[a] P. G. Ellison, L. W. Ward, C. Dobbe, S. A. Chavez, C. L. Atwood, C. L. Smith, L. M. Wolfram, J. L. Jones, L. N. Haney, and W. J. Reece, The Risk Significance of Induced Steam Generator Tube Rupture, INEL-95/0641, Rev. 1 (Draft), Lockheed Martin Idaho Technologies, Inc., Idaho National Engineering Laboratory, December 15, 1995.

[b] E. L. Fuller, M. A. Kenton, M. Epstein, R. E. Henry, and N. G. Cofie, Risks from Severe Accidents Involving Steam Generator Tube Leaks or Ruptures, EPRI TR-106194, Electric Power Research Institute, Palo Alto, CA (to be published).

for predicting failure of flawed and unflawed tubes is developed in the present paper. Predictions based on this model for high-temperature tests conducted at ANL under a variety of loading histories are much more in agreement with test results than those based on the flow stress models. However, for completeness, the flow stress models are also discussed in this paper.

Consider a tube with a flaw subjected to a temperature history T(t) and nominal hoop stress history $\sigma(t)$. To analyze the behavior of a tube under such a general loading history, both the flow stress and the creep rupture models make the following assumptions:

(1) The failure time and temperature of a flawed tube are the same as those of an unflawed tube subjected to a nominal hoop stress history $m_p\sigma(t)$ and the same temperature history T(t).

(2) The values of the magnification factor m_p determined from burst tests of flawed tubes at low temperatures are also applicable at high temperatures.

These assumptions may be valid for certain classes of creep and plasticity problems.[15] They are not strictly valid for the problem considered here, but the test program at ANL has shown that they can provide a reasonable approximation.

Flow stress models

In flow stress models, it is assumed that, for any arbitrary history of hoop stress $\sigma(t)$ and temperature T(t), failure of the remaining ligament occurs at a temperature T and nominal hoop stress σ whenever the following failure equation is satisfied, independent of stress-temperature history:

$$\sigma = \frac{\overline{\sigma(T)}}{m_p}, \tag{8}$$

where:

$\overline{\sigma(T)}$ is the flow stress at temperature T, and

m_p is a model-dependent hoop stress magnification factor that accounts for the crack (see Eqs. 2-4).

Flow stresses (computed with k = 0.5) for Alloy 600 from various sources[6, 7, 17,18] are plotted in Fig. 7a. Most of these tests were conducted under stroke-control at a nominal strain rate of 34%/min. Note that although there may be a wide variation in flow stress at low temperatures, the product form variations in the flow stress diminish rapidly with increasing temperature. Therefore, the INEL flow stress curve, which covers the widest range of temperature, is used for failure predictions. In Fig 7b, results from isothermal pressure ramp tests at two ramp rates are used to define "effective" flow stresses which are compared with the flow stress curve based on the INEL tensile tests. The rate-dependence of the flow stress is evident, and as expected, higher ramp rate leads to higher flow stress. Conceptually, it is possible to include rate effects within the framework of a flow stress model by generalizing the constitutive equation so that the flow stress is a function of both strain rate and temperature. In fact, several such constitutive relations based on the so-called equation of state theory are currently available (for example, see Ref. 16). However, in addition to being quite complex, they are not easily amenable to the problem of predicting failure of steam generator tubes, particularly those that contain flaws and are subjected to typical temperature and pressure histories expected during a severe accident. In this paper, the term flow stress models is used exclusively to denote simple rate-independent flow stress models. Because of their success at low temperatures, they were used initially to determine if they would provide reasonable failure predictions for the high-temperature tests of interest.

Creep rupture model

Creep failure of a uniaxially loaded specimen under a varying stress and temperature history can be predicted by a relatively straightforward analysis[15] and is often based on a linear time-fraction damage rule (e.g., Code Case N 47 of the ASME Code, Section III), as follows:

$$\int_0^{t_f} \frac{dt}{t_R(T,\sigma)} = 1 \tag{9}$$

where:

t_R is the time to creep rupture for a uniaxial specimen under a stress σ and temperature T, both of which may be functions of time, and

t_f is the time to failure.

A rigorous analysis of flawed tubes under a similar loading would be very complex. Therefore, the creep failure model was extended to flawed tubing using the assumptions referred to earlier, i.e., it was assumed that failure can be predicted by

$$\int_0^{t_f} \frac{dt}{t_R(T,m_p\sigma)} = 1 \tag{10}$$

To apply the creep rupture model for predicting failure under postulated severe accident conditions, creep rupture properties (particularly at short lives) of Alloy 600 tubes in the hoop direction are needed. Available creep rupture data (uniaxial tests) from the literature were collected and the following Larson-Miller representation for the data was established[a]:

$$t_R = 10^{\frac{P_{lm}}{T} - 15}, \tag{11a}$$

where:

T is in K and

the Larson-Miller parameter P_{lm} is defined in terms of the stress σ (in ksi) as follows:

$$P_{lm} = \begin{cases} 23.14 - 2.4\log_e(\sigma) \text{ for } \sigma \geq 5.7\,\text{ksi} \\ 24.18 - 3.0\log_e(\sigma) \text{ for } \sigma < 5.7\,\text{ksi} \end{cases} \tag{11b}$$

To establish the applicability of Eqs. 11a-b to our tubing material, constant-pressure creep-rupture tests were conducted on unflawed 22-mm (7/8-in.)-dia. tubes using both isothermal and constant temperature ramp loading. The experimental results are plotted in Fig. 8 against predicted times to failure, using Eqs. 11a-b. In all cases, the predicted times to failure are well within a factor of 2 (which is typical of the scatter in the uniaxial creep rupture data) of the experimental failure times, thus indicating that the above Larson-Miller representation of the data is adequate for our material.

Validation tests for the creep rupture model

To validate the creep rupture model, several types of tests were conducted on both flawed and unflawed steam generator tubes. The tests were conducted in a single zone furnace using programmable temperature and high pressure nitrogen gas to apply internal pressures on the tubes. A temperature profile measured transiently as well as steady state showed a maximum of 5°C axial variation within a central 50 mm (2 in) section with the center being the hottest. The maximum through thickness temperature gradient was less than 1°C. Tests were conducted on both unflawed and flawed tubing. The flaws were created

[a] W. J. Shack, Argonne National Laboratory, personal communication, 1996.

in the specimens using electro–discharge machining (EDM). Such notches are not as sharp as real cracks, but previous tests at lower temperatures have shown that there is very little effect of crack tip geometry on the failure loads.[6] At higher temperature the effect of the crack tip geometry would be expected to be of even less significance.

Isothermal failure tests

First, tests were conducted on flawed tubing by subjecting them to isothermal constant pressure loading. A summary of all the tests conducted to date together with the failure times predicted by the creep rupture model are given in Table 1. The predicted failure times using four different values of m_p are plotted against the experimental failure times in Fig. 9a for tubes containing a ≈ 60% deep, 25-mm (1 in.)-long crack. In addition to the diagonal perfect prediction line, Fig. 9a also shows differences of factor of 2 (which is typical of the scatter in the uniaxial creep rupture data) between the predicted and the observed times to failure by means of two additional lines. Except for a test at 667°C, the predicted failure times by the ANL m_p (Eq. 2c) are within a factor of 2 of the experimental failure times of the specimens. The predicted lives using m_p values as determined by the BCL (Eq. 2b) and EDF (Eq. 4a) equations are also reasonable, but those by the INEL equation (Eq.3b) underpredict the lives by more than a factor of 2 in most cases. It should be noted that the flow stress model is incapable of predicting time to failure for tests of this type and, in fact, would predict that none of the tubes should have failed.

Failure tests of specimens with deep cracks

There is some experimental evidence[5] that the numerical values of m_p computed by the BCL equation for short and deep cracks are too high for tests conducted at low temperatures where a flow stress model is valid. Results from tests, summarized in Table 2 and shown in Fig. 9b, confirm that this is also true at high temperatures. All the test specimens referred in this figure had ≥90% deep cracks. Note that the BCL equation grossly overestimates the damaging influence (i.e., underestimates the time to failure) of these cracks. The INEL and ANL equations do account for the less damaging influence of the deeper cracks than of the shallower cracks. Predictions by the EDF equation are not shown in Fig. 9b because at high temperatures, they are essentially the same as those by the BCL equation. At low temperatures the EDF model[5] predicts a smaller m_p for cracks that are more than 85% deep than the BCL model because the flow stress in the BCL equation is replaced by the ultimate tensile strength in the EDF equation (see Eq. 4b). However, there is little difference between the flow stress and the ultimate tensile strength at high temperatures because strain hardening is greatly reduced. Consequently, the EDF equation fails to account for the less damaging influence of deep cracks at high temperatures. Overall, the ANL correlation for m_p (Eq. 2c) gives the best predictions for failure times of specimens with shallow as well as deep cracks and is used for predicting failure of the rest of the high-temperature tests.

Pressure and temperature ramp tests

To evaluate the importance of loading rates on the failure conditions and compare the predictive capabilities of the creep rupture model and the flow stress model, two additional types of tests were conducted. In the first type, the specimens were heated to a temperature and then pressurized isothermally at a constant pressure ramp until failure. In the second type, the specimens were first pressurized at low temperature and then, with the pressure held constant, they were subjected to a constant temperature ramp until failure. A summary of all the tests of these types conducted to date together with the failure pressures and temperatures predicted by the creep rupture model are given in Tables 3-4. Results from both types of tests, plotted in Figs 6a and 6b, show that the loading rate (pressure or temperature), which is ignored in a simple flow stress model, has a significant influence even on the failure conditions of unflawed tubes. Note that the experimental results are closer to predictions of the creep rupture model than those of the flow stress model in all cases. For the tests at higher pressure ramp rate, the creep rupture model overestimates the failure pressures by a maximum of 25% whereas the flow stress model underestimates the failure pressures by as much as 50%. The failure temperatures for the temperature ramp tests are predicted almost exactly by the creep rupture model whereas the flow stress model can either underestimate or overstimate

the failure temperatures by 70°C. Fig 7b shows results from pressure ramp tests on flawed and unflawed tubes, clearly indicating that although the flow stress model would predict the failure pressures reasonably well for the lower ramp rate tests, it would underestimate the failure pressures at ≥ 800°C by almost a factor of 2 for the higher ramp rate tests if the INEL flow stress curve were used. The failure pressures are much closer to those predicted by the creep rupture model, see Fig. 10a. The pressures in the temperature ramp tests on flawed specimens were selected such that the product of m_p and the nominal hoop stresses were approximately equal for two crack geometries. Thus, the predicted failure temperatures for both geometries fall approximately on a single line for either the creep rupture or flow stress models, as shown in Fig. 10b. The experimental results are in much better agreement with the predictions of the creep rupture model and confirm that the effect of flaws on failure can be characterized by the m_p approach.

Failure tests for evaluating postulated severe accident time-temperature histories

Tests were performed at ANL to determine the behavior of flawed tubes under time/temperature histories that could be used to evaluate the failure of steam generator tubes under postulated severe accident conditions. An additional purpose of the tests was to provide further validation of the appropriate model to support its use to determine the time to failure of flawed tubes under time/temperature histories that could reach temperatures as high as 850°C.

In all the tests under this category, the internal pressure was held constant at 16 MPa (2.35 ksi). Tests were conducted on both 19 mm (3/4 in) and 22 mm (7/8 in) outer diameter tubes with wall thicknesses 1 mm (0.043 in) and 1.3 mm (0.050 in), respectively. Four different nominal flaw geometries with axial lengths 6 mm (0.25 in) , 25 mm (1 in.), and 50 mm (2 in) and depths varying from 20% to 65% of thickness were tested. The actual flaw depths were determined by fractography after the tests. In many cases, they were also measured prior to the tests by a replica technique. The differences between the two measurements, when available, were not large. Duplicate tests were run for all the 22 mm (7/8 in) diameter tube tests.

For the tests to date, two time/temperature histories have been considered. Both are based on preliminary analyses of an accident sequence involving total station blackout with a stuck-open steam generator secondary-side atmospheric dump valve, resulting in loss of feedwater and secondary-side depressurization. One, which is referred to as the "INEL ramp", is based on a preliminary analyses by INEL[a] and the other, referred to as the "EPRI ramp", is based on a preliminary analysis reported by EPRI[b]. The time-temperature scenarios calculated by INEL[a] and EPRI[b] for some postulated severe accident sequences are shown in Figs. 11a and 11b, respectively, which also show the time-temperature histories used in the ANL tests. In both series of tests the specimens were first heated rapidly to 300°C, equilibrated at 300°C, and then subjected to the test ramps. Both analyses also predict depressurization of the system due to the failure of the surge line. Because the primary purpose of our tests was to help develop a failure model, the tests have ignored the predicted depressurization. The EPRI analysis also predicts a reduction in temperature following a short 5 min. hold at 667°C. To increase the contribution of creep damage in the tests, the "EPRI" temperature history was arbitrarily modified to include a 2 h holdtime at 667°C and ignored the predicted reduction of temperature after the hold. If the specimen did not fail in 2 hours of constant temperature hold, it was subjected to a temperature ramp of 2°C/min. until failure. Neither ramp chosen for the tests was intended to be an accurate representation of a particular sequence, but together they can represent a range of histories for which a failure model would be needed. Thus, although the INEL and EPRI analyses predict that failure of the surge line nozzle and consequent depressurization of the system will occur prior to the failure of the steam generator tubes, the tests at ANL were continued with full pressure until failure occurred.

A summary of all the tests conducted to date together with the failure temperatures predicted by the creep rupture model are given in Tables 5 and 6. The experimental temperatures and times (above 300°C) to failure are compared with predicted

---

[a] P. G. Ellison, L. W. Ward, C. Dobbe. S. A. Chavez, C. L. Atwood, C. L. Smith, L. M. Wolfram, J. L. Jones, L. N. Haney, and W. J. Reece, The Risk Significance of Induced Steam Generator Tube Rupture, INEL-95/0641, Rev. 1 (Draft), Lockheed Martin Idaho Technologies, Inc., Idaho National Engineering Laboratory, December 15, 1995.

[b] E. L. Fuller, M. A. Kenton, M. Epstein, R. E. Henry, and N. G. Cofie, Risks from Severe Accidents Involving Steam Generator Tube Leaks or Ruptures, EPRI TR-106194, Electric Power Research Institute, Palo Alto, CA (to be published).

failure temperatures and times in Figs. 12a and 12b, respectively. The predicted values were calculated with the creep rupture model by using the Larson-Miller parameter, Eq. 11a-b, and the stress magnification factor (Eq. 2c). In most cases, predicted times (above 300°C) and temperatures are quite close to the experimentally observed values.

Similar comparisons for the flow stress model predictions are shown in Figs. 13 a-b. The predicted values were calculated with the INEL flow stress curve (Fig. 7a) and the stress magnification factor (Eq. 2c). Note that the failure temperatures and times (above 300°C) for the tests using the INEL ramp were underpredicted significantly. The accurate prediction of the EPRI ramp tests was probably a fortuitous consequence of the average strain rates in the ligament being close to the strain rate used in the tensile tests from which the flow stress curve was derived.

It is evident that the creep rupture model not only provides more accurate predictions of the failure loadings than the flow stress models but also accounts for loading rate effects. Therefore, the creep rupture model can be expected to predict failure under varying temperature and pressure histories during postulated severe accidents more reliably than a simple rate-independent flow stress model.

Conclusions

Available flow stress models for predicting failure of flawed steam generator tubing under normal operating conditions and design basis accidents have been reviewed. All the models predict similar failure pressure for shallow axial cracks, but give significantly different failure pressures when the cracks are deep. A new correlation developed under this study using the PNNL data from earlier studies appears to correlate data for all flaw depths better than the existing ones. The new correlation is supported by detailed finite-element analysis.

The failure pressure for tubes containing unsymmetrical circumferential cracks has recently been observed experimentally to increase in the presence of lateral constraint. Detailed finite-element analyses show that such behavior is to be expected and that a tube support plate spacing of 0.65 m (26 in.) or less should increase the failure pressure to almost that of a fully constrained tube.

Tests conducted on unflawed and flawed specimens at the high temperatures postulated for severe accidents show that the failure pressure at a constant temperature is dependent on the pressure ramp rate and that the failure temperature at a constant pressure is dependent on the temperature ramp rate. While rate-independent flow stress model cannot predict such a behavior, the creep rupture model developed under this study can do so.

The creep rupture model has been validated with failure tests on flawed specimens under a variety of loading histories. While the flow stress model is incapable of predicting the time to failure of flawed specimen under isothermal, constant pressure loading, the creep rupture model can do so. Finally, the creep rupture model can predict failure times and temperatures of both flawed and unflawed tubes subjected to varying temperature and pressure histories more accurately than the flow stress models.

Acknowledgment

The author would like to acknowledge helpful discussions with Drs. W. J. Shack and D. R. Diercks of Argonne National Laboratory and Dr. J. Muscara of the U. S. Nuclear Regulatory Commission. Thanks are also due to Messrs. J. Franklin and L. Knoblich for conducting the high-temperature failure tests and to Mr. K. Mruk for providing the measured crack parameters. This work was supported by the Office of Nuclear Regulatory Research, U.S.Nuclear Regulatory Commission.

References

1. G. T. Hahn, M. Sarrate, and A. R. Rosenfield, "Criteria for crack extension in cylindrical pressure vessels," *Int. J. Fracture Mech.*, Vol. **5**, No. 3, 1969.

2. F. Erdogan, "Ductile failure theories for pressurized pipes and containers," *Int. J. of Pres. Ves. & Piping*, Vol. **4**, 1976.

3. R. J. Eiber, W. A. Maxey, A. R. Duffy, and T. J. Atterbury, "Investigation of the Initiation and Extent of Ductile Pipe Rupture," BMI–1908, Battelle Memorial Institute, June 1971.

4. J. F. Kiefner, W. A. Maxey, R. J. Eiber, and A. R. Duffy, "Failure stress levels of flaws in pressurized cylinders," in *Progress in Flaw Growth and Fracture Toughness Testing*, Kaufman, J. G., Natil. Symp. on Fracture Mechanics (6th : 1972 : Philadelphia), American Society for Testing and Materials, Committee E–24 on Fracture Testing of Metals, American Society for Testing and Materials, ASTM Special Technical Publication 536, Philadelphia, 1973.

5. B. Flesch and B. Cochet, "Crack stability criteria in steam generator tubes," *Int. Cong. on Pressure Vessel Technology*, Beijing, Sept. 1988.

6. R. J. Kurtz, R. A. Clark, L. R. Bradley, W. M. Bowen, P. G. Doctor, R. H. Ferris, and F. A. Simonen, *Steam Generator Tube Integrity Program/Steam Generator Group Project, Final Project Summary Report*, NUREG/CR–5117, PNNL, Richland, WA, May 1990.

7. S. A. Chavez, C. L. Atwood, P. G. Ellison, and J. L. Jones, "Estimating structural failure frequency of degraded steam generator tubes," Submitted to ASME.

8. S. Ranganath and H. S. Mehta, "Engineering Methods for the Assessment of Ductile Fracture Margin in Nuclear Power Plant Piping," Elastic Plastic Fracture 2nd Symp., Vol. 2, Fracture Resistance Curves and Engineering Applications, American Society for Testing and Materials, ASTM Special Technical Publication 803, Philadelphia, 1983.

9. M. F., Kanninen, A. Zahoor, G. M. Wilkowski, I. Abou–Sayed, C. Marschall, D. Broek, S. Sampath, C. Rhee, and J. Ahmad, "Instability Predictions for Circumferential Cracked Type 304 Stainless Steel Pipes under Dynamic Loading," EPRI NP–2347 (Vol.1: Summary; Vol. 2: A lices), Electric Power Research Institute, Palo Alto, CA, April 1982.

10. K. Hasegawa, T. Shimizu, and S. Shida, Consideration of Allowable Flaw Size for Pressurized Pipes, *Nucl. Eng. and Design*, Vol. 87, 1985.

11. R. Kurihara, S. Ueda, and D. Sturm, Estimation of the Ductile Unstable Fracture of Pipe with a Circumferential Surface Crack Subjected to Bending, *Nucl. Eng. and Design*, Vol. 106, 1988.

12. B. Cochet, J. Engstrom, and B. Flesch, "PWR steam generator tube and tube support plate plugging criteria," Paper 4.1, *Steam generator tubes mechanical, LBRB, and probabilistic studies*, EDF, France, 1990.

13. P. Hernalsteen, "Structural and Leakage Integrity of Tubes Affected by Circumferential Cracking," presented at NEA/CNRA/CSNI Int. Workshop on Steam Generator Integrity in Nuclear Power Plants, Oak Brook, IL, Oct. 30-Nov. 2, 1995.

14. B. Cochet and B. Flesch, "Application of the leak before break concept to steam generator tubes," SMIRT-9, Vol. D, Lausanne, Switzerland, 1987.

15. I. Finnie and W. R. Heller, *Creep of Engineering Materials*, New York, McGraw-Hill, 1959.

16. E. W. Hart, "A phenomenological theory for plastic deformation of polycrystalline metals," Acta Met., Vol. 18, 1970.

17. J. L. Rempe, S. A. Chavez, G. L. Thinnes, C. M. Allison, G. E. Korth, R. J. Witt, J. J. Sienicki, S. K. Wang, L.A. Stickler, C. H. Heath, and S. D. Snow, *"Light Water Reactor Lower Head Failure Analysis,"* NUREG/CR-5642, EGG-2618, I.N.E.L, Idaho Falls, ID, Oct., 1993.

18. International Nickel Co., "Engineering Properties of Inconel Alloy 600," Tech. Bull. T-7, 1964.

Table 1 *Constant-pressure rupture tests at various temperatures on specimens with and without flaws to validate m_p approach. Also shown are the predicted failure times by the ANL creep rupture model.*

Test	Crack Geometry			Loading History		Failure Conditions			
No.	2c (in.)	a/h	m_p	T	p	T_f	p_f	t_f	Pred. t_f
T-37	1	0.59	1.96	Ramp to 667°C and hold	Constant 2350 psi	667°C	2350 psi	336 min.	128 min.
T-56[a]	1	0.65	2.21	Ramp to 667°C and hold	Constant 2350 psi	667°C	2350 psi	74 min.	62 min.
T-38	1	0.62	2.07	Ramp to 700°C and hold	Constant 1915 psi	700°C	1915 psi	28 min.	88 min.
T-41	Unflawed		1	Ramp to 700°C and hold	Constant 4500 psi	700°C	4500 psi[b]	38 min.	42 min.
T-61[c]	Unflawed		1	Ramp to 700°C and hold	Constant 4450 psi	700°C	4450 psi	49 min.	45 min.
T-47	1	0.55	1.82	Ramp to 750°C and hold	Constant 1400 psi	750°C	1400 psi	186 min.	176 min.
T-60	Unflawed		1	Ramp to 750°C and hold	Constant 3290 psi	750°C	3290 psi	29 min.	43 min.
T-48	1	0.55	1.82	Ramp to 800°C and hold	Constant 1400 psi	800°C	1400 psi	26 min.	32 min.
T-42	Unflawed		1	Ramp to 800°C and hold	Constant 2350 psi	800°C	2350 psi	33 min.	50 min.

[a] Duplicate of test listed immediately above.

[b] Pressure decreased gradually from 4750 psi to 4250 psi during hold.

[c] Duplicate of test listed immediately above, but with pressure held constant at 4450 psi during hold.

Table 2 *Constant-pressure failure tests with deep cracks to validate the new m_p correlation proposed by ANL. Also shown are the predicted failure times by the ANL creep rupture model.*

Test	Crack Geometry			Loading History		Failure Conditions			
No.	2c (in.)	a/h	m_p	T	p	T_f	p_f	t_f	Pred. t_f
T-55	0.25	0.91	2.45	Ramp in 1h to 800°C, then pressurize and hold	Constant 750 psi	800°C	750 psi	420 min.	180 min.
T-78[a]	0.25	0.92	2.61	Ramp to 800°C and hold	Constant 750 psi	800°C	750 psi	246 min.	130 min.
T-83	Unflawed		1	Ramp to 800°C and hold	Constant 1800 psi	800°C	1800	228 min.	202 min.
T-72	1	0.92	7.62	Ramp to 800°C and hold	Constant 356 psi	800°C	356 psi	19 min.	23 min.
T-84	1	0.91	6.85	Ramp to 800°C and hold	Constant 450 psi	800°C	450 psi	2 min	18 min.
T-87	Unflawed		1	Ramp to 800°C and hold	Constant 2910 psi	800°C	2910 psi	12 min.	15 min.
T-66	2	0.90	7.83	Ramp to 800°C and hold	Constant 300 psi	800°C	300 psi	23 min.	15 min.
T-85	Unflawed		1	Ramp to 800°C and hold	Constant 3000 psi	800°C	3000 psi	10 min.	13 min.

[a] Duplicate of test listed immediately above.

Table 3 *Constant-pressure temperature ramp tests to validate creep rupture model. Also shown are the predicted failure temperatures by the ANL creep rupture model.*

Test	Crack Geometry			Loading History		Failure Conditions	
No.	2c (in.)	a/h	m_p	T	p	T_f	Pred. T_f
T-62	Unflawed		1	Ramp to 600°C in 1 h, then 20°C/min	Constant 2350 psi	913°C	916°C
T-63	Unflawed		1	Ramp at 2°C/min	Constant 2350 psi	843°C	838°C
T-71	Unflawed		1	Ramp at 0.2°C/min	Constant 2350 psi	779°C	770°C
T-67	1	0.65	2.21	Ramp at 20°C/min	Constant 1065 psi	892°C	916°C
T-68	1	0.65	2.21	Ramp at 0.2°C/min	Constant 1065 psi	770°C	778°C
T-74	1	0.93	8.60	Ramp at 0.2°C/min	Constant 270 psi	860°C	918°C
T-73	1	0.93	8.60	Ramp at 0.2°C/min	Constant 1065 psi	612°C	604°C
T-76	0.25	0.89	2.22	Ramp at 20°C/min	Constant 1090 psi	915°C	911°C
T-77	0.25	0.9	2.32	Ramp at 0.2°C/min	Constant 1040 psi	778°C	766°C
T-59	2	0.79	3.93	Ramp at 2°C/min	Constant 750 psi	810°C	801°C
T-79	2	0.92	9.68	Ramp at 0.2°C/min	Constant 245 psi	815°C	914°C
T-80[a]	2	0.92	9.68	Ramp at 0.2°C/min	Constant 245 psi	859°C	914°C
T-81	2	0.93	10.99	Ramp at 0.2°C/min	Constant 217 psi	678°C	768°C

[a] Duplicate of test listed immediately above.

Table 4 *Isothermal pressure ramp tests to establish the maximum flow stress curve. Also shown are the predicted failure pressures and times by the ANL creep rupture model.*

Test	Crack Geometry			Loading History		Failure Conditions			
No.	2c (in.)	a/h	m_p	T	p	p_f	t_f	Pred. p_f	Pred. t_f
T-35	Unflawed		1	840°C (isothermal)	Ramped at 2300 psi/min. to 3000 psi and hold	3000 psi	3.3 min.	3000 psi	5.8 min.
T-36	Unflawed		1	840°C (isothermal)	Ramped at 2300 psi/min. to 4000 psi and hold	4000 psi	1.8 min.	4000 psi	2.8 min.
T-46	Unflawed		1	840°C (isothermal)	Ramped at 2300 psi/min	4190 psi	1.8 min.	4987 psi	2.2 min.
T-45	Unflawed		1	840°C (isothermal)	Ramped at 230 psi/min	3090 psi	13 min.	3390 psi	15 min.
T-86	Unflawed		1	800°C (isothermal)	Ramped at 230 psi/min	3730 psi	16 min.	4115 psi	18 min.
T-82	Unflawed		1	800°C (isothermal)	Ramped at 2300 psi/min to 4800 psi and hold	4800 psi	2.2 min.	4800 psi	3.4 min.
T-57	0.25	0.75	1.58	800°C (isothermal)	Ramped at 2300 psi/min	3520 psi	1.5 min.	3520 psi	1.8 min.
T-58	1	0.79	3.32	800°C (isothermal)	Ramped at 2300 psi/min	1590 psi	0.7 min.	2194 psi	0.9 min.
T-70	1	0.65	2.21	840°C (isothermal)	Ramped at 2300 psi/min	2250 psi	1.0 min.	2570 psi	1.1 min.
T-69	1	0.65	2.21	800°C (isothermal)	Ramped at 2300 psi/min	2740 psi	1.2 min.	3020 psi	1.3 min.
T-75	1	0.65	2.21	700°C (isothermal)	Ramped at 2300 psi/min	3370 psi	1.5 min.	4860 psi	2.1 min.

Table 5 *Flaw sizes and temperatures at failure for INEL ramp tests. Also shown are the predicted failure temperatures by the ANL creep rupture model.*

	3/4 in. diameter tube				7/8 in. diameter tube			
2c (in.)	Test No.	a/h	T_f	Pred. T_f	Test No.	a/h	T_f	Pred. T_f
Unflawed	T-2	Unflawed	823°C	837°C	T-10	Unflawed	835°C	844°C
Unflawed	T-13	Unflawed	826°C	837°C	T-30	Unflawed	843°C	844°C
0.25	T-12	0.59	798°C	806°C	T-7	0.65	803°C	806°C
0.25	-	-	-	-	T-34	0.62	802°C	809°C
1	T-11	0.61	758°C	752°C	T-9	0.54	768°C	784°C
1	-	-	-	-	T-33	0.54	778°C	792°C
2	T-3	0.45	774°C	788°C	T-6	0.36	808°C	805°C
2	T-14	0.35	805°C	803°C	T-32	0.41	800°C	803°C
2	T-4	0.2	808°C	816°C	T-5	0.16	825°C	824°C
2	-	-	-	-	T-31	0.22	817°C	818°C

Table 6 *Flaw sizes and temperatures at failure for EPRI ramp tests. Also shown are the predicted failure temperatures by the ANL creep rupture model.*

	3/4 in. diameter tube				7/8 in. diameter tube			
2c (in.)	Test No.	a/h	T_f	Pred. T_f	Test No.	a/h	T_f	Pred. T_f
Unflawed	T-22	Unflawed	828°C	833°C	T-19	Unflawed	839°C	842°C
Unflawed	-	-	-	-	T-28	Unflawed	843°C	842°C
0.25	T-23	0.57	767°C	772°C	T-18	0.66	779°C	786°C
0.25		-	-	-	T-24	0.66	781°C	782°C
1	T-29	0.54	726°C	702°C	T-16	0.57	724°C	692°C
1	-	-	-	-	T-27	0.55	724°C	727°C
2	T-21	0.40	760°C	745°C	T-15	0.30	794°C	786°C
2	-	-	-	-	T-26	0.41	770°C	762°C
2	T-20	0.12	814°C	814°C	T-17	0.20	816°C	802°C
2	-	-	-	-	T-25	0.21	817°C	811°C

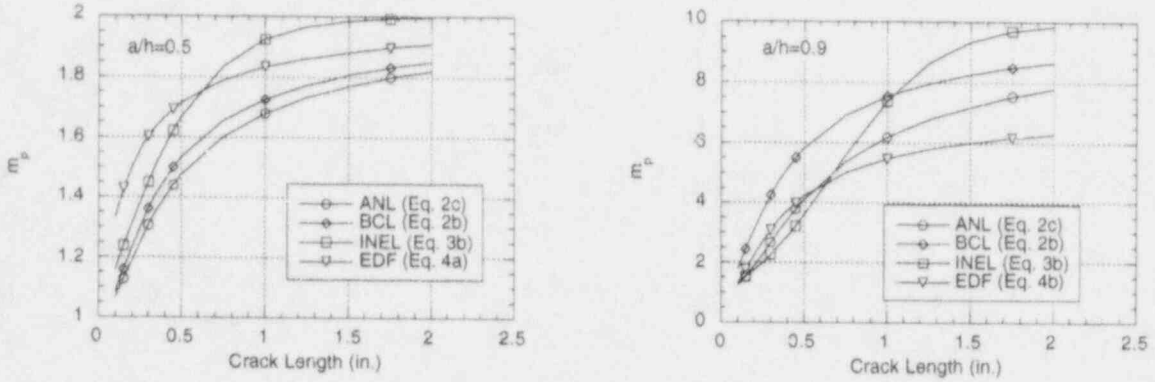

(a) (b)

Fig. 1 *Magnification factor m_p as computed by BCL (Kiefner et al.) equation (Eq. 2b), ANL (Shack) equation (Eq. 2c), INEL (Chavez et al.) equation (Eq. 3b), and the EDF (Flesch and Cochet) equation (Eqs. 4a-b) as a function of crack length for crack depth-to-thickness ratios (a) a/h=0.5 and (b) a/h=0.9.*

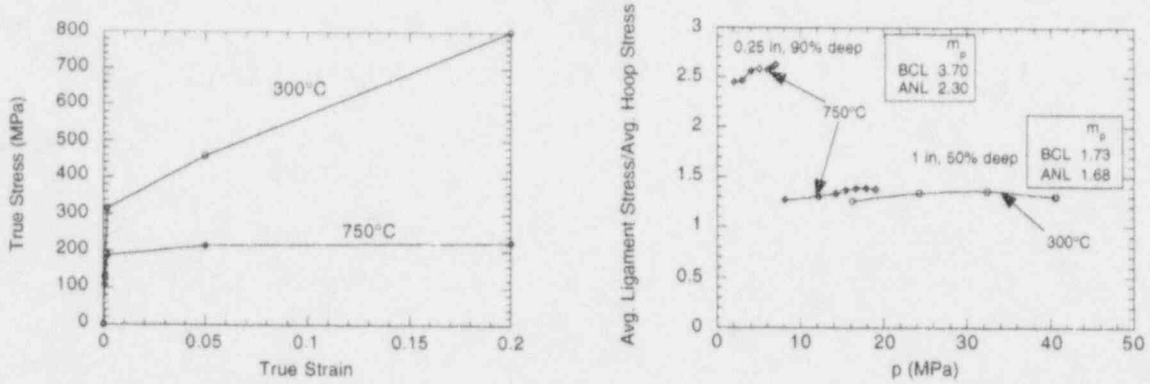

(a) (b)

Fig. 2 *(a) True stress-strain curve used in finite-element analysis and (b) variation of calculated hoop stress enhancement factor in the ligament with pressure for a 22 mm (7/8 in.) dia. tube with two axial part-through crack geometries at 300 and 750°C.*

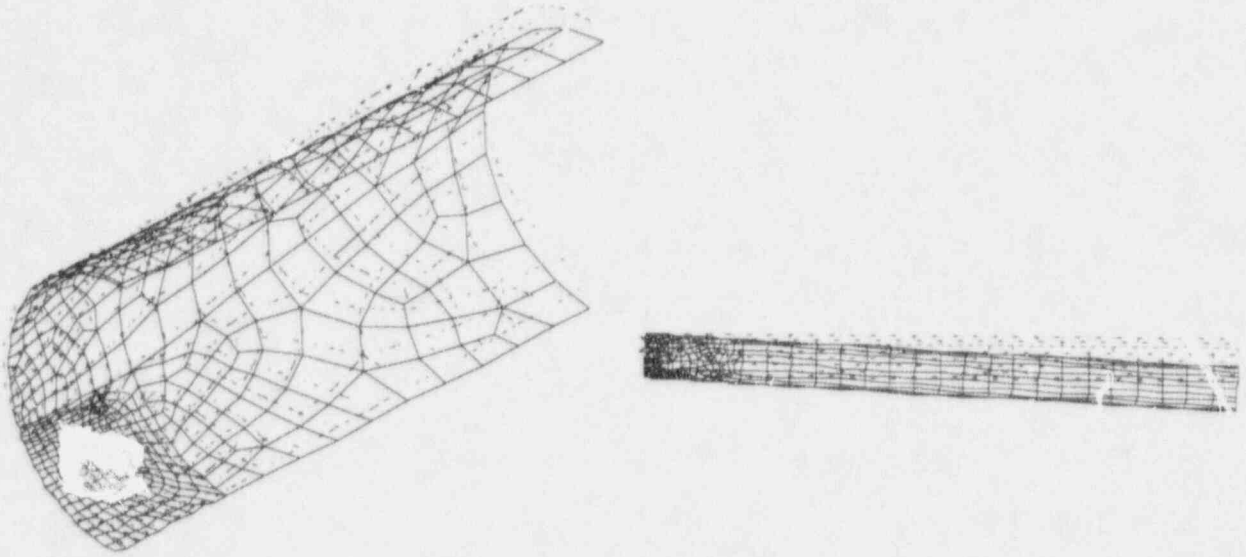

(a) (b)

Fig. 3 *(a) Typical near-tip finite-element model for tube with a through wall circumferential crack; (b) typical displaced shape of tube for free-bending case.*

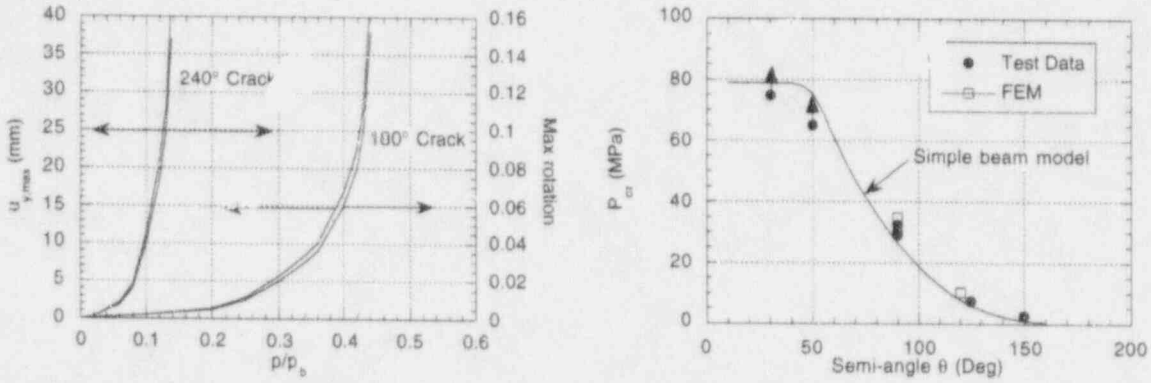

(a) (b)

Fig. 4 *(a) Variations of free end displacements and maximum rotations with normalized burst pressure for tubes with 240° and 180° through-wall circumferential cracks. (b) Comparison of experimental burst pressure data with predicted burst pressures using a simplified beam model and finite-element method.*

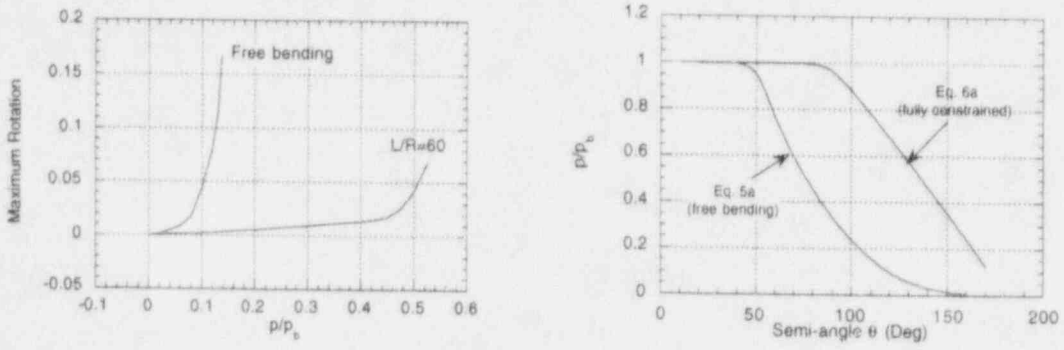

(a) (b)

Fig. 5 *(a) Maximum rotation of section of 22 mm (7/8 in.) dia. tube containing a 240° circumferential crack when free to bend and when supported laterally at a span of 0.67 m (26 in.) and (b) variation of critical burst pressure with semi-angle of crack for free-bending and fully constrained cases.*

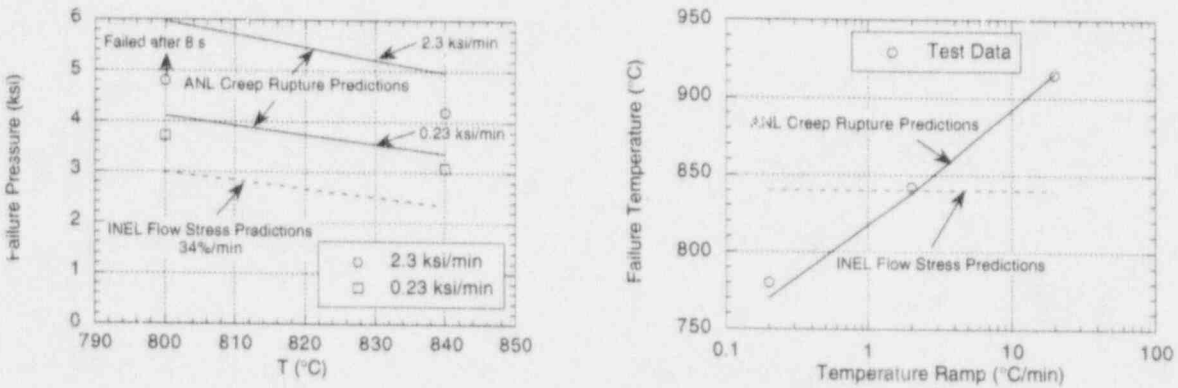

(a) (b)

Fig.6 *Effects of (a) loading rate on failure pressure in isothermal burst test and (b) temperature ramp on failure temperature in burst test at a constant pressure of 16 MPa (2.35 ksi) of unflawed 22 mm (7/8 in.) dia. Inco 600 tube. Also shown are predicted failure pressures and temperatures by flow stress model (dashed lines) using INELflow stress curve and by ANL creep rupture model (solid lines).*

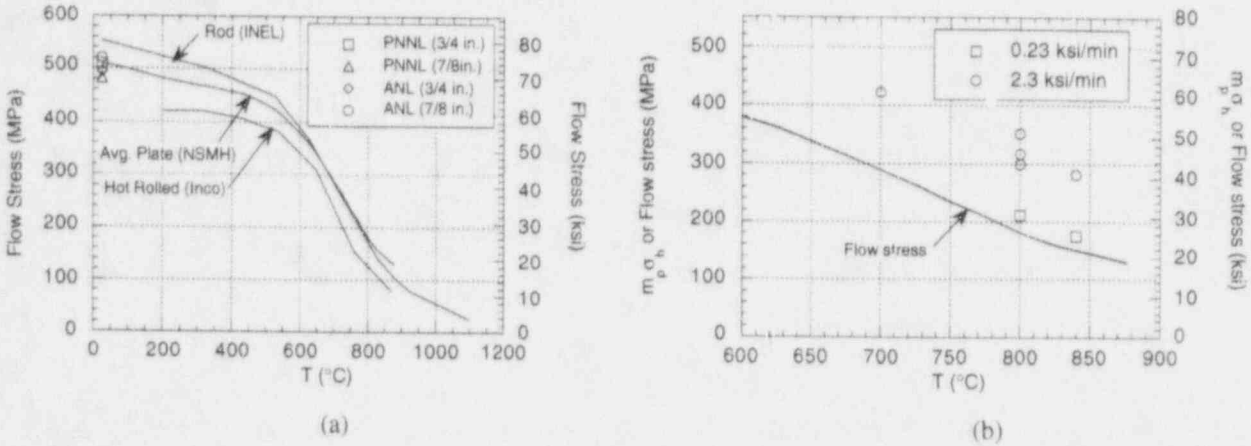

Fig. 7 *(a) Flow stress for various product forms of Inco 600 as a function of temperature. (b) Comparison of flow stress curve with those obtained experimentally by pressure ramp tests on flawed and unflawed tubes.*

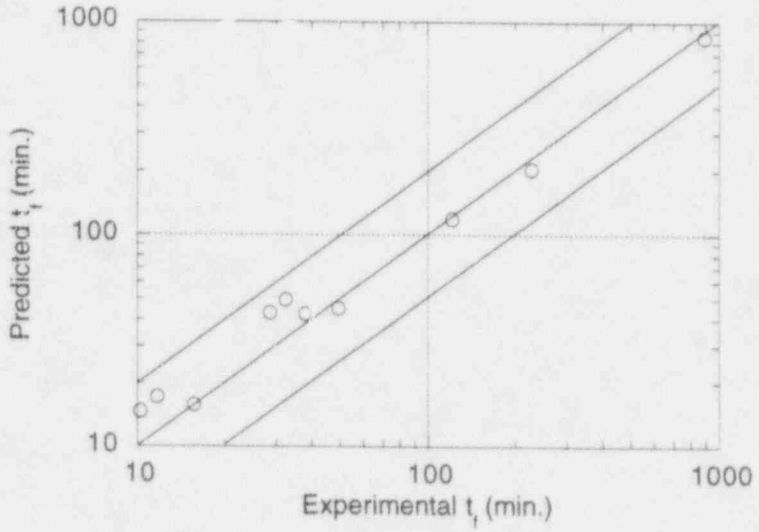

Fig. 8 *Comparison of experimental and predicted times to failure of unflawed Inco 600 tubing under constant internal pressure. Tests were conducted isothermally and under constant temperature ramps of 0.2°C/min., 2°C/min., and 20°C/min.*

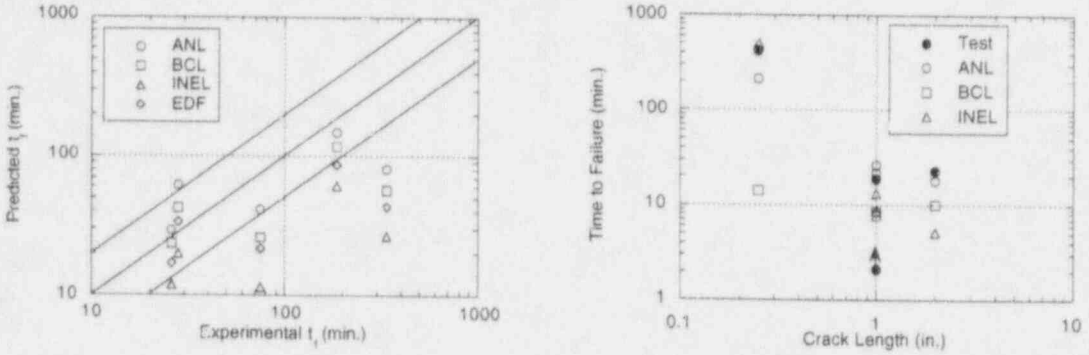

Fig. 9 *Comparison of experimental and predicted times to failure of flawed Inco 600 tubing tested isothermally under constant internal pressure, for (a) shallow flaws of length of 25 mm (1 in.) and depths ranging from 56% to 65% and at temperatures between 667°C and 800°C and (b) deep flaws with depths between 90% and 92% at a temperature of 800°C. Arrow indicates pin hole failure in which pressure was undiminished after failure, but the test was interrupted.*

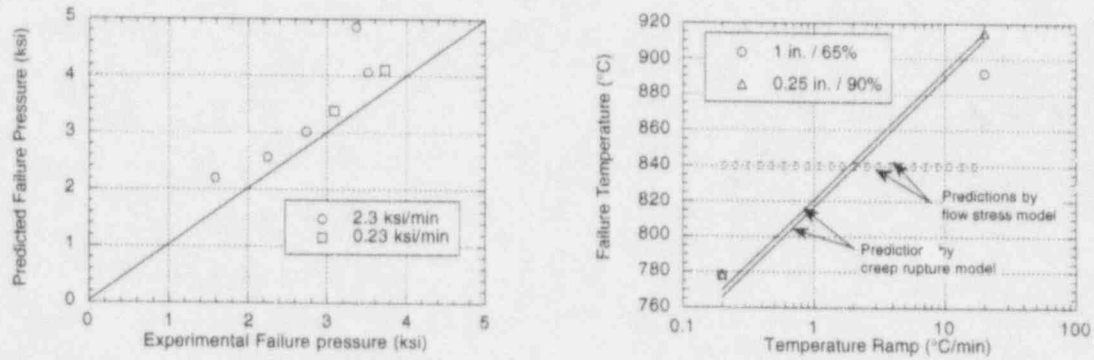

Fig. 10 *Comparison of experimental and predicted (a) failure pressures of flawed and unflawed tubes subjected to two pressure ramps isothermally at 700 - 840°C and (b) failure temperatures of flawed tubes subjected to two temperature ramps with constant internal pressures chosen such that the product of m_p and nominal hoop stress were kept approximately constant.*

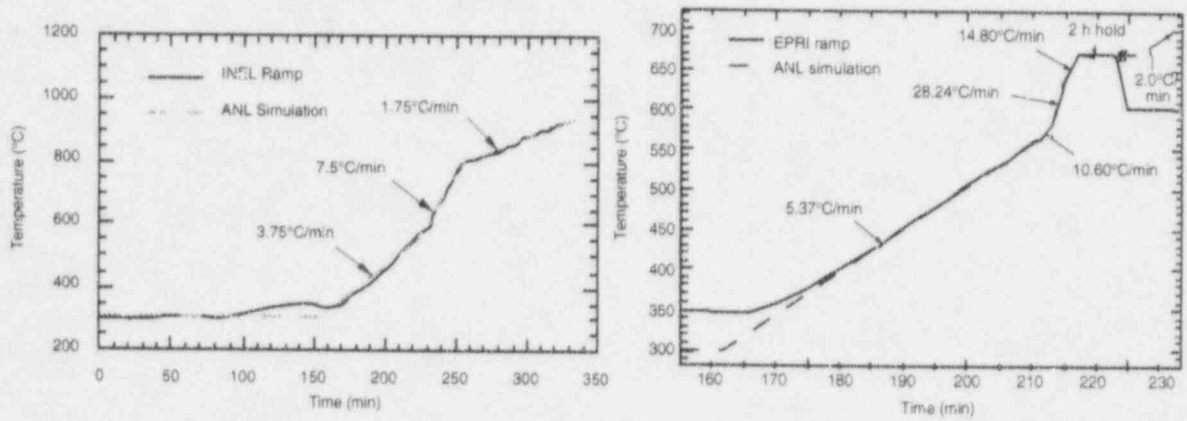

Fig. 11 Calculated and ANL simulation of (a) INEL ramp and (b) EPRI ramp for high-temperature tests.

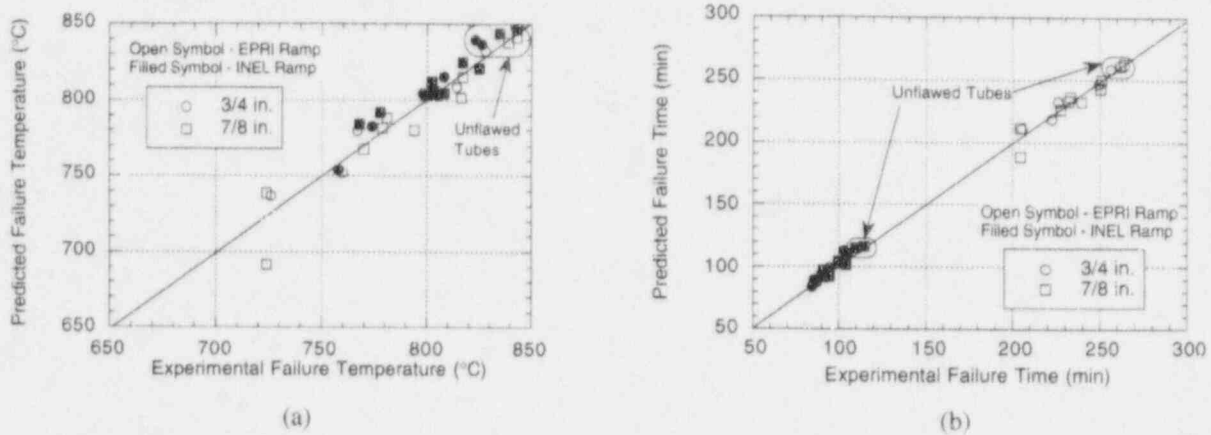

(a) (b)

Fig. 12 Comparison of predicted (by creep rupture model) versus observed (a) failure temperatures and (b) times (above 300°C) to failure for high-temperature failure tests conducted with the INEL and EPRI temperature ramps.

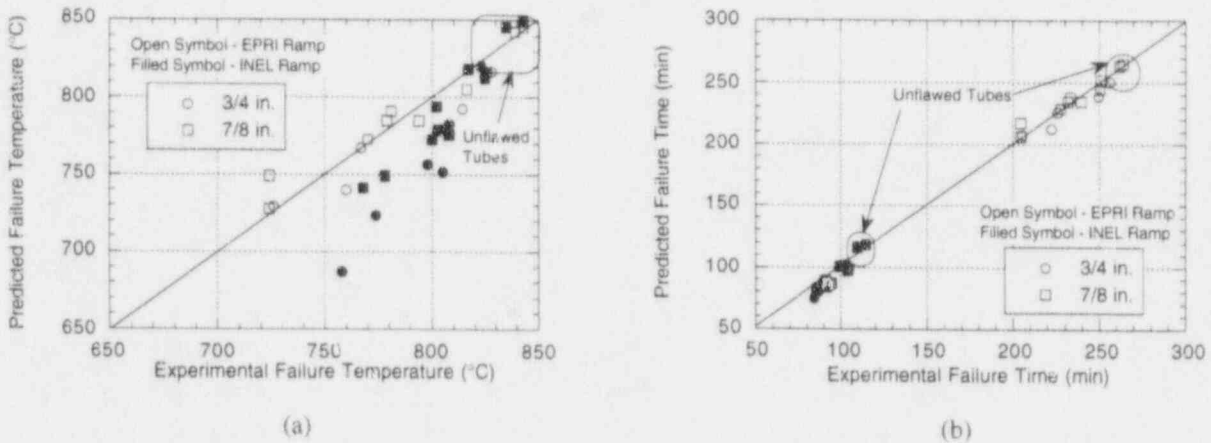

(a) (b)

Fig. 13 Comparison of predicted (by flow stress model) versus observed (a) failure temperatures and (b) times (above 300°C) to failure for high-temperature failure tests conducted with the INEL and EPRI temperature ramps.